mathematics

Article

Analysis of Noise-Induced Transitions in a Thermo-Kinetic Model of the Autocatalytic Trigger

Irina Bashkirtseva *, Makar Pavletsov, Tatyana Perevalova and Lev Ryashko

Institute of Natural Sciences and Mathematics, Ural Federal University, Lenina 51, 620000 Ekaterinburg, Russia; makar.pavletsov@urfu.ru (M.P.); tatyana.perevalova@urfu.ru (T.P.); lev.ryashko@urfu.ru (L.R.)
* Correspondence: irina.bashkirtseva@urfu.ru

Abstract: Motivated by the increasingly important role of mathematical modeling and computer-aided analysis in engineering applications, we consider the problem of the mathematical modeling and computer-aided analysis of complex stochastic processes in thermo-kinetics. We study a mathematical model of the dynamic interaction of reagent concentration and temperature in autocatalysis. For the deterministic variant of this model, mono- and bistability parameter zones as well as local and global bifurcations are revealed, and we show how random multiplicative disturbances can deform coexisting equilibrium regimes. In a study of noise-induced transitions, we apply direct numerical simulation and an analytical approach based on the stochastic sensitivity technique. Two variants of bistability with different scenarios of stochastic transformations are studied and compared.

Keywords: noise-induced transitions; stochastic sensitivity; thermo-kinetic model; autocatalytic trigger

MSC: 37H10; 37H20

check for updates

Citation: Bashkirtseva, I.; Pavletsov, M.; Perevalova, T.; Ryashko, L. Analysis of Noise-Induced Transitions in a Thermo-Kinetic Model of the Autocatalytic Trigger. *Mathematics* **2023**, *11*, 4302. https://doi.org/10.3390/math11204302

Academic Editor: Song-Kyoo (Amang) Kim

Received: 15 September 2023
Revised: 7 October 2023
Accepted: 12 October 2023
Published: 16 October 2023

1. Introduction

In modern branches of the natural sciences and engineering applications, mathematical modeling and computer-aided analysis play an increasingly important role. In the wide range of these studies, the complex dynamic regimes of thermo-kinetics have attracted the attention of many researchers [1–3]. In experimental findings, a diversity of operation modes, both steady-state and oscillatory, were revealed. Understanding of the internal mechanisms of such regimes and their transformations can be achieved by thorough analysis of adequate mathematical models (see, e.g., [3–6]). Due to the strong nonlinearity, thermo-kinetic models are multistable and highly sensitive to parameter changes and random disturbances [7]. Progress in the investigation of such nonlinear dynamic models can be ensured by a combination of the modern methods of analytical mathematics [8], bifurcation theory [9,10], and high-precision numerical simulation [11–15].

Nowadays, various mathematical models of the thermo-chemical processes are actively studied (see [3] and bibliography therein). In a variety of thermo-chemical processes, autocatalytic reactions are of particular interest [16–18]. It is known that heterogeneous catalytic reactions can occur with significant thermal effects. Therefore, it is important to study the dynamic properties of processes on the catalyst surface, taking into account changes in its temperature. In this case, the combination of nonlinearity in the temperature and kinetic feedbacks leads to a significant complication of the dynamic processes.

As is known, the random disturbances that are inevitably present in nonlinear systems can cause unexpected phenomena such as noise-induced transitions [19,20], stochastic bifurcations [21], noise-induced excitement [22], stochastic and coherence resonance [23], etc. When studying these phenomena, time-consuming direct numerical simulation is usually used. In stochastic systems, an exhaustive description of the dynamics of probabilistic distributions is given by the Fokker–Planck Equation [24]. However, direct use of this equation encounters serious mathematical difficulties even in two-dimensional cases, so asymptotics and approximations are helpful [25,26]. Among others, the stochastic sensitivity function technique is a useful constructive tool for studying phenomena caused by noise (see, e.g., [27–33]).

In this paper, as an initial deterministic skeleton, we consider the two-dimensional thermo-kinetic model proposed in [16]. Its peculiarity is that the kinetic subsystem is an autocatalytic trigger: for the same set of parameters the model exhibits a coexistence of several equilibrium modes. This model was used as a basis for understanding the complex dynamics of thermo-kinetic processes on the catalyst surface. A parametric description of the dynamic modes of this deterministic model was initiated in [17,18].

The purpose of this paper is to study how random disturbances in this model can deform deterministic dynamics and generate new operating modes in thermo-kinetics of autocatalytic processes. The rest of the paper is structured as follows. In Section 2, we study two variants of bistability in the deterministic system. Despite having a common feature, namely the coexistence of two stable equilibria, these variants have significantly different bifurcation scenarios. Such a difference manifests itself in the presence of random disturbances. In Section 3, we study stochastic phenomena caused by noise-induced transitions between equilibria. In this analysis, we use the methods of direct numerical simulation of solutions of stochastic equations with the subsequent statistical processing as well as the mathematical approach based on the stochastic sensitivity technique and apparatus of confidence domains.

2. Deterministic Model

It is well known that many critical phenomena in thermo-chemical processes are associated with multistability. The reason for this multistability is the specific interplay of temperature and kinetic nonlinearities. The presence of coexisting attractors dramatically complicates the behavior of the system under conditions of random disturbances.

In this paper, we will study these critical phenomena on the basis of a thermo-kinetic model of an autocatalytic trigger on the catalyst surface, first proposed in [16]:

$$\begin{aligned} \dot{x} &= k_1(1-x) - xf(y) - k_2x(1-x)^2, \\ \dot{y} &= \beta x f(y) + s(1-y). \end{aligned} \tag{1}$$

Here, the variables x and y are dimensionless measures of concentration and temperature, respectively. The function $f(y) = De^{\gamma(1-\frac{1}{y})}$ describes the temperature dependence of the reaction rate. Here, γ is the activation parameter and D is the Damköhler number. The dimensionless parameters k_1, k_2, β, and s are all positive.

In this paper, following [3], we fix

$$\beta = 0.375,\ s = 2,\ k_2 = 0.6.$$

We will describe two bifurcation scenarios that prevail in model (1) for two sets of fixed parameters: $k_2 = 2.5$, $\gamma = 55$ (case 1) and $k_2 = 1$, $\gamma = 75$ (case 2). The coefficient D is considered as a bifurcation parameter. These two scenarios correspond to the possible coexistence of two stable equilibria, but differ, firstly, in the location of the equilibria on the phase plane, and secondly, in the complexity of the observed bifurcations.

The equilibria of model (1) are solutions of the following transcendental equation:

$$\beta D x e^{\gamma\left(1-\frac{1}{y(x)}\right)} + s(1-y(x)) = 0. \tag{2}$$

Here, $y(x) = 1 + \frac{\beta}{s}(k_1 - k_2x(1-x))(1-x)$. With the chosen parameter values, this equation can have up to three solutions. Next, we analyze the existence and stability of the equilibria of the model (1) for the selected cases with D being a bifurcation parameter. We will call the equilibria M_i ($i = 1, 2, 3$), where i increases with increasing value of variable x.

2.1. Case 1: $k_2 = 2.5$, $\gamma = 55$

Figure 1 shows the bifurcation diagram and Lyapunov exponents of the equilibria of the model (1) with a change in the parameter D. In the interval $D \in (0, D_1)$ ($D_1 = 0.03323$), there are two stable equilibria M_1 (green) and M_3 (blue), and one saddle equilibrium M_2 (red dashed). At the bifurcation point $D_1 = 0.03323$, a saddle-node bifurcation occurs, which means that the two equilibria M_2 and M_3 collide and disappear. Furthermore, for $D > D_1$, only one stable equilibrium M_1 exists. In Figure 1b, the Lyapunov exponents show that both stable equilibria are nodes, i.e., both Lyapunov exponents for each equilibria are negative. At the bifurcation point D_1, the Lyapunov exponents for M_2 and M_3 are equal, which corresponds to the occurrence of the saddle-node bifurcation.

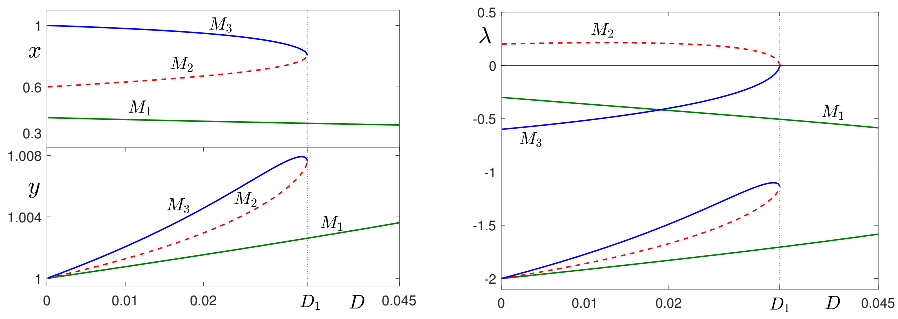

(**a**) (**b**)

Figure 1. System (1) with $k_2 = 2.5$, $\gamma = 55$: (**a**) coordinates, x (top) and y (bottom), of the equilibria M_1 (green), M_2 (red dashed), and M_3 (blue). Here, M_1 and M_3 are stable nodes and M_2 is a saddle. In (**b**), the Lyapunov exponents are shown by the corresponding colors.

In Figure 2, we show phase portraits of the model (1) for $D = 0.02$ (Figure 2a) and $D = 0.04$ (Figure 2b). In Figure 2a, one can observe a coexistence of two stable nodes $M_1 = (0.376486, 1.00154)$ (filled green circle) and $M_3 = (0.949131, 1.00457)$ (filled blue circle). The stable manifold (dashed red line) of the saddle $M_2 = (0.6708, 1.00296)$ (empty red circle) creates the boundary between the basins of attraction of the two stable equilibria M_1 and M_3.

In this case, a bistable scenario occurs in model (1). Depending on the initial condition, a solution can converge to one equilibrium state or the other. It should be mentioned that the equilibrium regimes M_1 and M_3 have almost the same temperature, but the concentration differs twice. Figure 2b exemplifies the monostable regime with only one equilibrium $M_1 = (0.356612, 1.00318)$ (filled green circle). This means that all solutions converge to only one state with a lower value of concentration.

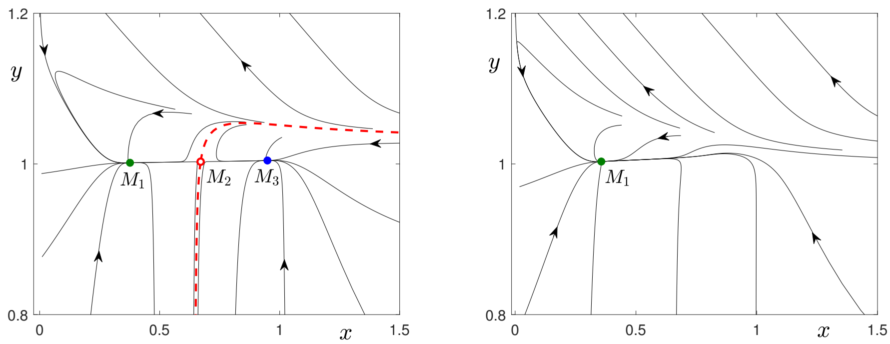

(**a**) (**b**)

Figure 2. Phase portraits of the system (1) with $k_2 = 2.5$, $\gamma = 55$ for: (**a**) $D = 0.02$ and (**b**) $D = 0.04$. Here, M_1 (filled green circle) and M_3 (filled blue circle) are stable nodes, and M_2 (empty red circle) is a saddle. Here, the separatrix shown by the red dashed line is the stable manifold of the saddle M_2. Arrows show evolution over time.

In the following section, we consider a more complex bifurcation scenario.

2.2. Case 2: $k_2 = 1$, $\gamma = 75$

In this case, the dynamical behavior of model (1) differs from the previous case and appears to be more complicated. There are also only up to three equilibria, but the stable equilibria that exist reflect the dynamics not only for different values of concentration, but also for different temperature levels. An additional complication is related to the emerging new bifurcation scenario. For this case, all bifurcation values of the parameter D are presented below:

$$\begin{array}{cccc} D_1 = 0.01176245 & D_2 = 0.01178143 & D_3 = 0.01211245 & D_4 = 0.01586245 \\ D_5 = 0.0243 & D_6 = 0.03262665 & D_7 = 0.033195 & D_8 = 0.0335. \end{array}$$

Figure 3 shows the bifurcation diagram and Lyapunov exponents of the equilibria of model (1) with $k_2 = 1$, $\gamma = 75$ and changing parameter D. In the interval $D \in (0, D_1)$, there is only one stable equilibrium M_3 (blue). At the bifurcation point D_1, a saddle-node bifurcation occurs, which means that two equilibria M_1 (green) and M_2 (red) appear. Here, the Lyapunov exponents presented in Figure 3c provide more information.

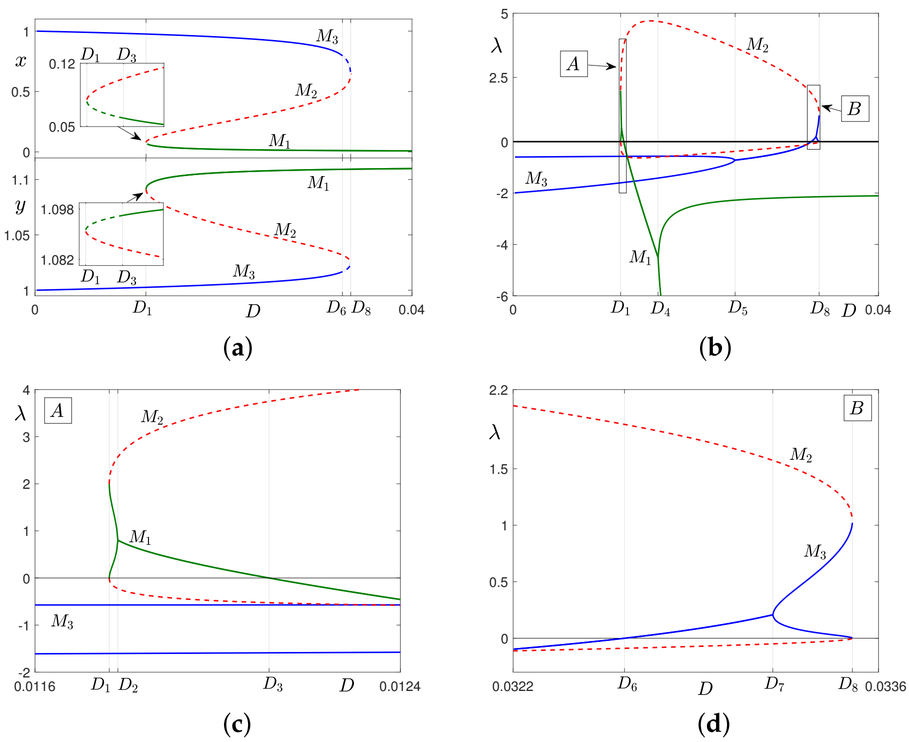

Figure 3. System (1) with $k_2 = 1$, $\gamma = 75$: (**a**) coordinates, x (top) and y (bottom), of the equilibria M_1 (green), M_2 (red dashed), and M_3 (blue). In (**b**–**d**), the Lyapunov exponents are shown by the corresponding colors.

First, at $D = D_1$, the equilibrium M_1 is born as an unstable node: both Lyapunov exponents are real and positive. At $D = D_2$, the Lyapunov exponents for M_1 become complex and the real part stays positive up to $D = D_3$, so M_1 is an unstable focus. At $D = D_3$, the real part becomes negative and remains so until the Lyapunov exponents become real again at $D = D_4$, i.e., M_1 is a stable focus (see Figure 3b). For $D > D_4$, Lyapunov exponents are real and negative, so M_1 is a stable node. At the same time, the Lyapunov exponents for the equilibrium M_2 have different signs in the parameter interval $D_1 < D < D_8$, so M_2 is a saddle.

As for M_3, this equilibrium is a stable node in the interval $0 < D < D_5$, where both its Lyapunov exponents are real and negative (see Figure 3b). At $D = D_5$, the Lyapunov exponents become complex and the real part stays negative up to $D = D_6$, so M_3 is a stable focus. At $D = D_6$, the real part becomes positive and remains so until the Lyapunov exponents become real again at $D = D_7$, i.e., M_3 is an unstable focus (see Figure 3d). In the interval $D_7 < D < D_8$, the Lyapunov exponents are both real and positive, so M_3 is an unstable node. At the bifurcation value D_8, a saddle-node bifurcation occurs, which means that the two equilibria M_2 and M_3 collide and disappear. Furthermore, for $D > D_8$, only one stable equilibrium M_1 exists.

Thus, in this case, model (1) demonstrates bistable behavior in the interval $D_3 < D < D_6$. Although in the intervals $D_1 < D < D_3$ and $D_6 < D < D_8$ there are three equilibria, there is only attracting one.

In Figure 4, we show the phase portraits of model (1) for different parameter zones. Figure 4a shows the dynamic regime for $D = 0.008$ with only one equilibrium $M_3 = (0.984734, 1.00167)$ (filled blue circle); this is a stable node. All trajectories converge to M_3, which corresponds the attractive state with the higher concentration and lower temperature. It is worth noting that there are different types of transient process at play: one type of transient is formed by solutions converging immediately to equilibrium, the other first makes an ascent at the temperature and then with lower concentration converge to the equilibrium. This convergence behavior we observe while M_3 exists.

In Figure 4b for $D = 0.0119$, a phase portrait with three equilibria is plotted. Here, $M_1 = (0.066023, 1.09427)$ (empty green circle) is an unstable focus, $M_2 = (0.0931766, 1.08765)$ (empty red circle) is a saddle, and $M_3 = (0.975423, 1.00265)$ (filled blue circle) is a stable node. The stable manifold (dashed red line) of the saddle M_2 creates a boundary between the two types of transients mentioned above.

Figure 4c exemplifies a coexistence of two stable equilibria for $D = 0.013$: $M_1 = (0.0463086, 1.09939)$ (stable focus, filled green circle) and $M_3 = (0.972488, 1.00296)$ (stable node, filled blue circle). The stable manifold (dashed red line) of the saddle $M_2 = (0.128324, 0.128324)$ (empty red circle) is a separatrix between the basins of attraction of the two stable equilibria M_1 and M_3. So, in this case, model (2) is bistable. Depending on the initial condition, the solution can converge to one equilibrium state or the other: one with a lower temperature and higher concentration, the other with a higher temperature and lower concentration.

In Figure 4d for $D = 0.02$, a coexistence of two stable nodes, $M_1 = (0.0209389, 1.10638)$ (filled green circle) and $M_3 = (0.948999, 1.00527)$ (filled blue circle), and the saddle $M_2 = (0.246123, 1.05858)$ (empty red circle) is presented. The dynamical behavior is similar to one shown in Figure 4c with the difference being in the asymptotic behavior of M_1 (node instead of focus).

Figure 4e shows another slightly different scenario for $D = 0.03$ of the coexistence of two stable equilibria, $M_1 = (0.0122653, 1.10888)$ (filled green circle) and $M_3 = (0.873089, 1.01164)$ (filled blue circle), and the saddle $M_2 = (0.420613, 1.03871)$ (empty red circle). Here, M_1 is a stable node while M_3 is a stable focus.

In Figure 4f for $D = 0.033$, the equilibrium $M_1 = (0.0109274, 1.10927)$ (filled green circle) is a stable node, $M_2 = (0.545091, 0.545091)$ (empty red circle) is a saddle, and $M_3 = (0.766769, 1.01842)$ (empty blue circle) is an unstable focus. By the red dashed line, we show the stable manifold of the saddle M_2 that creates a boundary between two types of the transient behavior.

Figure 4g shows the dynamic regime for $D = 0.04$ with only one equilibrium $M_1 = (0.00871817, 1.10991)$ (filled green circle); this is a stable node. This means that all solutions of the system (1) converge to only one state with lower value of concentration and with higher temperatures.

To summarize, this thermo-kinetic model exhibits a diversity of complex dynamic regimes even in the deterministic case. In the next section, we will consider additional effects caused by random disturbances.

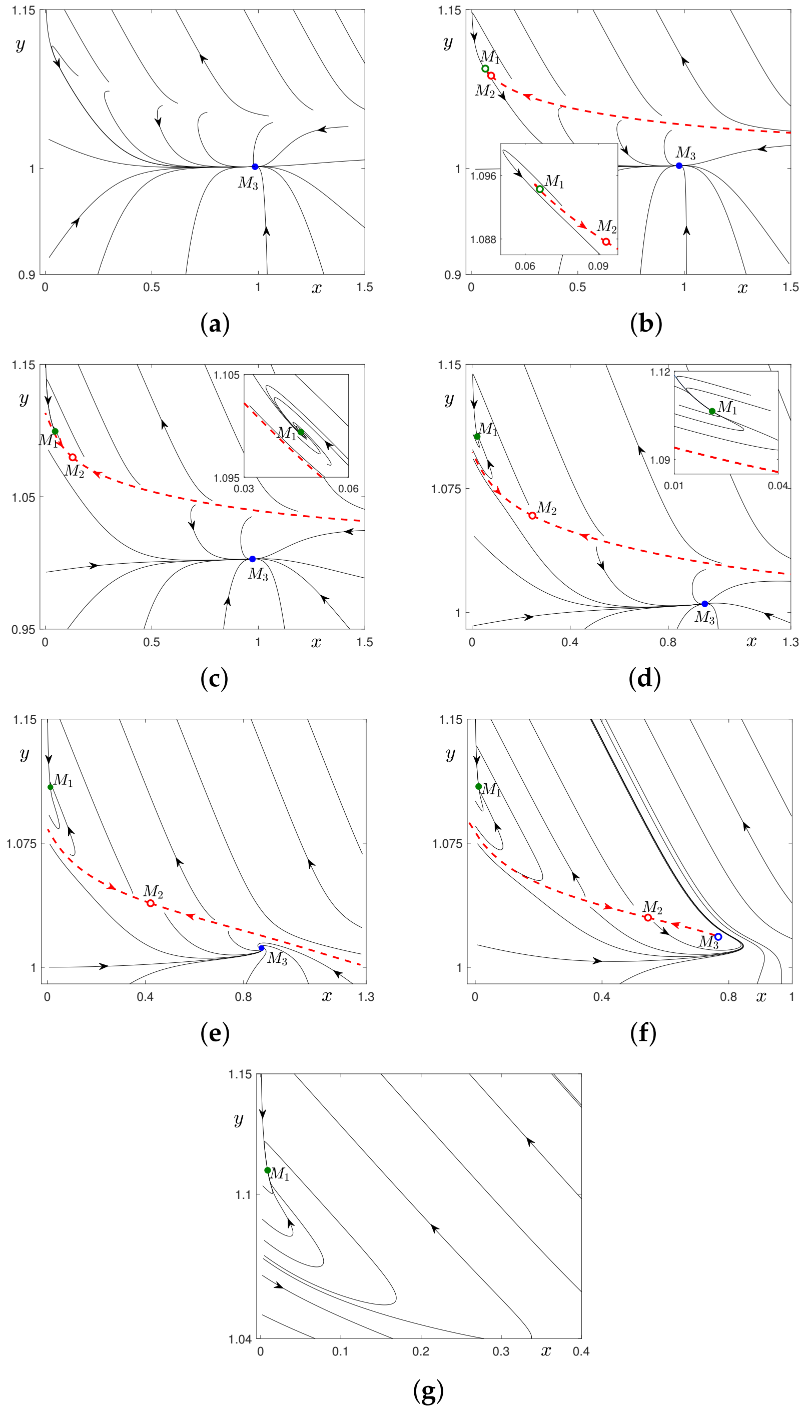

Figure 4. Phase portraits of model (1) with $k_2 = 1$, $\gamma = 75$ for: (**a**) $D = 0.008$, (**b**) $D = 0.0119$, (**c**) $D = 0.013$, (**d**) $D = 0.02$, (**e**) $D = 0.03$, (**f**) $D = 0.033$, and (**g**) $D = 0.04$. The equilibria M_1, M_2, and M_3 are shown by green, red, and blue, respectively. Here, the separatrix shown by a red dashed line is the stable manifold of the saddle M_2. Arrows show evolution over time.

3. Stochastic Model

Let us consider a stochastic version of the thermo-kinetic model with multiplicative random disturbances:

$$\begin{aligned} \dot{x} &= k_1(1-x) - xf(y) - k_2x(1-x)^2 + \varepsilon x\xi(t), \\ \dot{y} &= \beta xf(y) + s(1-y). \end{aligned} \tag{3}$$

Here, $\xi(t)$ is a scalar white Gaussian noise with parameters $\mathrm{E}\xi(t) = 0$, $\mathrm{E}\xi(t)\xi(\tau) = \delta(t-\tau)$, and ε is the noise intensity. In stochastic simulation of random solutions of the system (3), we use the Euler–Maruyama scheme with the time step 0.001.

3.1. Stochastic Effects in the Case 1 with $k_2 = 2.5$, $\gamma = 55$

First, we consider the bistability parameter range $0 < D < D_1 = 0.03323$ where deterministic system (1) has two stable equilibria (see Section 2.1). For $D = 0.02$, Figure 5a shows the x- and y-coordinates of random solutions of system (3) starting at M_1 (green) and M_3 (blue) versus noise intensity. Here and further, we use the following colors designation: if the trajectory starts at the equilibrium M_1 (M_3) then random states (Figures 5a and 6a), mean values (Figures 5b and 6b), time series (Figures 7 and 8), and probability (Figures 9 and 10) are plotted in green (blue). First, the dispersion of random states around both equilibria increases. For $\varepsilon \approx 0.05$, solutions starting at M_3 (blue) begin to transit to M_1. For $\varepsilon > 0.1$, a reverse transition from the equilibrium M_1 to the basin of M_3 begins to be observed. The results of the statistical analysis of these stochastic transformations are shown in Figure 5b in terms of mean values m_x, m_y versus noise intensity. For noise intensity $\varepsilon < 0.04$, two mean values differ. With a further increase in ε, the mean values of random solutions starting at M_3 (blue) rapidly decrease and merge with the mean values of random solutions starting at M_1 (green). After such a merging, the mean values slowly increase.

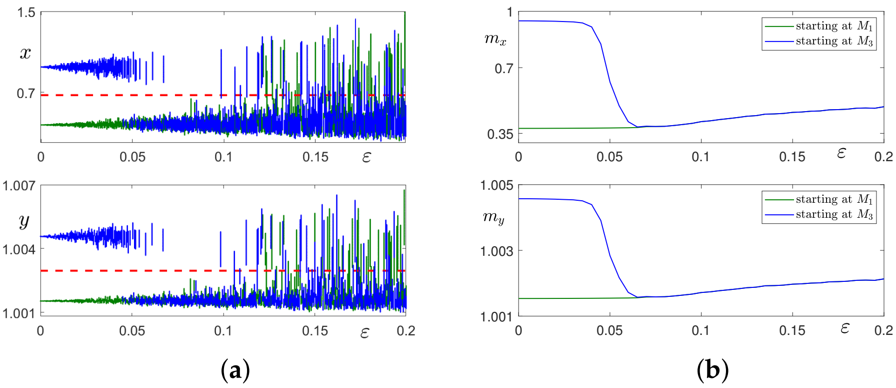

Figure 5. Stochastic system (3) with $k_2 = 2.5$, $\gamma = 55$, $D = 0.02$: (**a**) random states of solutions starting at M_1 (green) and M_3 (blue); (**b**) corresponding mean values. Here, red dashed lines mark coordinates of the equilibrium M_2.

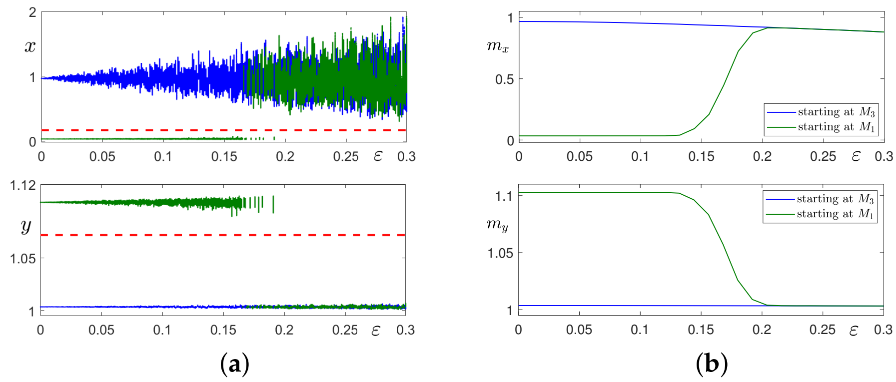

Figure 6. Stochastic system (3) with $k_2 = 1$, $\gamma = 75$, $D = 0.015$: (**a**) random states of solutions starting at M_1 (green) and M_3 (blue); (**b**) corresponding mean values. Here, red dashed lines mark coordinates of the equilibrium M_2.

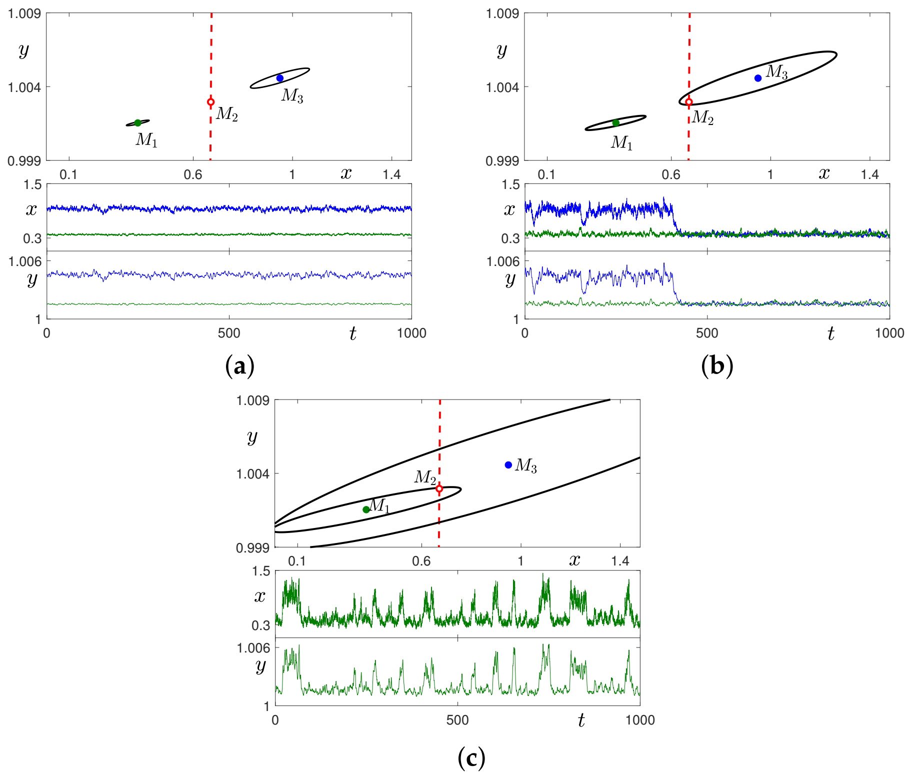

Figure 7. Noise-induced transitions in system (3) with $k_2 = 2.5$, $\gamma = 55$, $D = 0.02$ between equilibria M_1 (green circle) and M_3 (blue circle): (**a**) no transition for $\varepsilon = 0.03$, (**b**) transition $M_3 \to M_1$ for $\varepsilon = 0.08$, (**c**) transitions $M_1 \leftrightarrow M_3$ for $\varepsilon = 0.25$. Here, red dashed lines mark the separatrices. In top panels, we show equilibria and confidence ellipses. In bottom panels, we show time series of solutions starting at M_1/M_3 in green/blue.

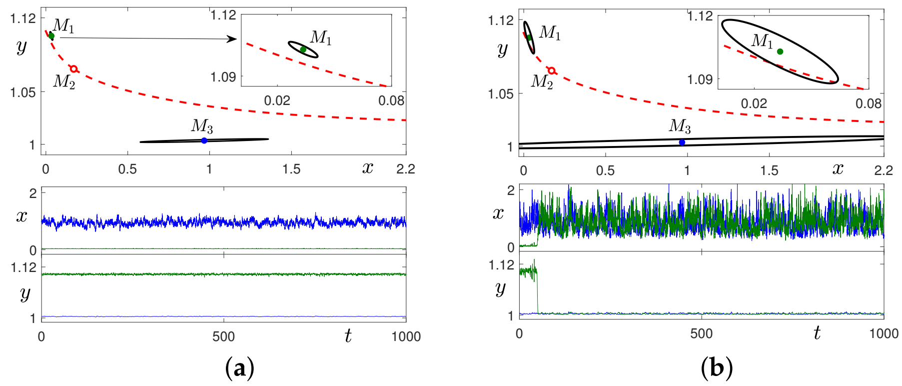

Figure 8. Noise-induced transitions in stochastic system (3) with $k_2 = 1$, $\gamma = 75$, $D = 0.015$: (**a**) no transition for $\varepsilon = 0.1$, (**b**) transition from M_1 (green circle) to M_3 (blue circle) for $\varepsilon = 0.4$. Here, red dashed lines mark the separatrices. In top panels, we show equilibria and confidence ellipses. In bottom panels, we show time series of solutions starting at M_1/M_3 in green/blue.

In order to give a parametric description of the observed noise-induced transitions, we will use the stochastic sensitivity function technique [27–31]. This technique was introduced for constructive approximation of the probabilistic distribution of random states in the neighborhood of the deterministic attractor. The stochastic sensitivity function technique was first elaborated for continuous-time systems and now covers cases of such attractors as equilibria, limit cycles, and tori [27,30,31,34]. Moreover, for discrete-time systems, the theory of stochastic sensitivity was elaborated also for closed invariant curves [35] and chaotic attractors [36]. This theory is effectively used in the stochastic analysis of nonlinear dynamic models in various fields of science (see, e.g., [33,37–39]), and also in control problems [40,41].

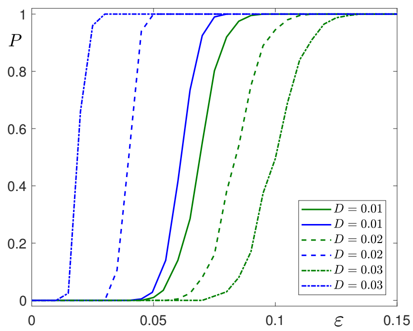

Figure 9. Probability $P(\varepsilon)$ of noise-induced transitions in system (3) with $k_2 = 2.5$, $\gamma = 55$ for different values of the parameter D: $M_3 \to M_1$ (blue) and $M_1 \to M_3$ (green).

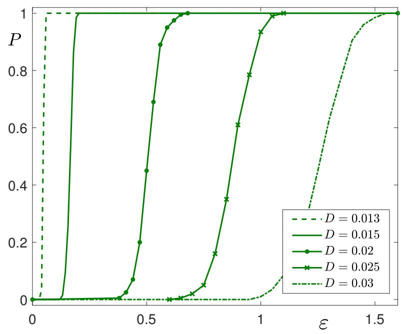

Figure 10. Probability of noise-induced transitions $M_1 \to M_3$ in stochastic system (3) with $k_2 = 1$, $\gamma = 75$.

Geometrically, the stochastic sensitivity function technique can be applied in the form of confidence domains [29,32]. Such domains calculated by this technique allow one to get a clear spatial description of the random states' dispersion near the deterministic attractor.

For the stable equilibrium $M(\bar{x}, \bar{y})$ of the two-dimensional stochastic system, a dispersion of random states can be approximated by a confidence ellipse

$$\frac{z_1^2}{\mu_1} + \frac{z_2^2}{\mu_2} = -2\varepsilon^2 \ln(1 - \mathcal{P}),$$

where parameters $\mu_1 > \mu_2$ are eigenvalues of the stochastic sensitivity matrix W, variables z_1 and z_2 are coordinates of this ellipse in the basis of orthonormal eigenvectors u_1, u_2 of the matrix W, the parameter ε is the noise intensity, and $\mathcal{P}$ stands for the fiducial probability.

So, when constructing the confidence ellipse, one has to calculate the stochastic sensitivity matrix W. This matrix is a unique solution of the algebraic Equation [28]

$$JW + WJ^\top + G = 0, \tag{4}$$

where J is a Jacobi matrix of the original deterministic system at the equilibrium point $M(\bar{x}, \bar{y})$ and the matrix G reflects an influence of the random disturbances. For the system (3), we have

$$J(x,y) = \begin{bmatrix} -k_1 - De^{\gamma(1-\frac{1}{y})} - k_2(1 - 4x + 3x^2) & -\gamma D \dfrac{x}{y^2} e^{\gamma(1-\frac{1}{y})} \\ \beta De^{\gamma(1-\frac{1}{y})} & \beta\gamma D \dfrac{x}{y^2} e^{\gamma(1-\frac{1}{y})} - s \end{bmatrix},$$

$$G(x) = \mathrm{diag}[x^2, 0].$$

The stochastic sensitivity matrix W allows one to approximate the covariance matrix of solutions $(x^{\varepsilon}(t), y^{\varepsilon}(t))$ of the stochastic system near the equilibrium $M(\bar{x}, \bar{y})$:

$$cov(x^{\varepsilon}(t), y^{\varepsilon}(t)) \approx \varepsilon^2 W.$$

Spatial peculiarities of the dispersion of random solutions $(x^{\varepsilon}(t), y^{\varepsilon}(t))$ near the equilibrium $M(\bar{x}, \bar{y})$ are reflected by eigenvalues and eigenvectors of the matrix W. Indeed, eigenvalues μ_1, μ_2 of the stochastic sensitivity matrix W define the eccentricity and size of the confidence ellipse in directions of eigenvectors u_1, u_2. Note that the extent of the ellipse is proportional to the noise intensity ε.

So, the spectral characteristics of the matrix W make it possible to obtain an approximation of the probability density near the equilibrium in the Gaussian form:

$$\rho(z_1, z_2) = Ke^{-\dfrac{z_1^2}{2\mu_1\varepsilon^2} - \dfrac{z_2^2}{2\mu_2\varepsilon^2}}.$$

Consider how this stochastic sensitivity technique can be used in analysis of the noise-induced transitions in system (3). In Figure 11a, eigenvalues μ_1 (solid) and μ_2 (dashed) $(\mu_1 > \mu_2 > 0)$ of the stochastic sensitivity matrix of equilibria M_1 (green) and M_3 (blue) are plotted versus parameter D. Note that both eigenvalues for M_3 are bigger then the eigenvalues for M_1. This means that the dispersion of stochastic states around the equilibrium M_3 would be wider. The largest eigenvalue μ_1 of the stochastic sensitivity matrix for the equilibrium M_3 increases sharply when parameter D approaches the bifurcation value D_1, while the value of μ_1 for the equilibrium M_1 slightly decreases with an increase in parameter D. Figure 11b shows an example of the confidence ellipse around the equilibrium M_3 for $D = 0.02$ and noise intensity $\varepsilon = 0.01$ constructed using the stochastic sensitivity matrix. Note that dispersion of random states (grey) is well approximated by this ellipse.

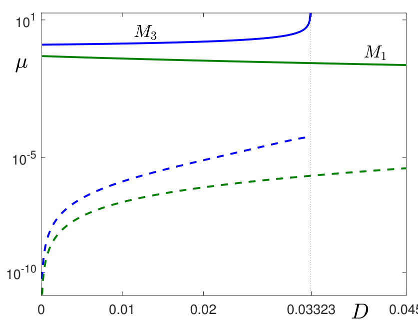

(**a**)

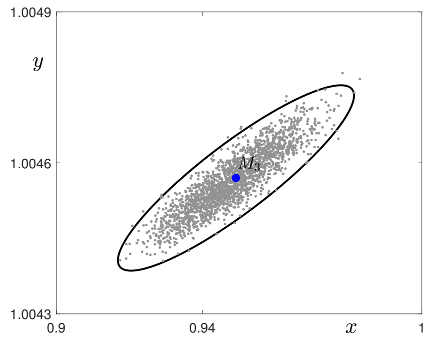

(**b**)

Figure 11. Stochastic sensitivity of equilibria M_1 and M_3 in system (3) with $k_2 = 2.5$, $\gamma = 55$: (**a**) eigenvalues μ_1 (solid) and μ_2 (dashed) $(\mu_1 > \mu_2 > 0)$ of the stochastic sensitivity matrix W of equilibria M_1 (green) and M_3 (blue), (**b**) confidence ellipse (black) and stochastic states (grey) for the equilibrium M_3 (blue) with $D = 0.02$ and noise intensity $\varepsilon = 0.01$.

The relative position of the confidence ellipses and the boundary of the basin of attraction of a deterministic attractor makes it possible to describe noise-induced transitions. Figure 7 demonstrates an application of this method. For the noise intensity $\varepsilon = 0.03$ in Figure 7a (top), confidence ellipses (black) for both equilibria lie far from the separatrix (red dashed line) between the basins of attraction of the equilibria M_1 and M_3. This means that random states are localized near M_1 or M_3, and transitions do not occur. This behavior is shown by the time series in Figure 7a (bottom).

In Figure 7b (top), for $\varepsilon = 0.08$, one of the confidence ellipses, related to equilibrium M_3, crosses the boundary of the basins of attraction. This indicates the occurrence of a noise-induced transition from M_3 to M_1, which is shown in the time series below. The situation where both ellipses cross the separatrix is presented for $\varepsilon = 0.25$ in Figure 7c (top). In this case, we observe noise-induced two-way transitions between two equilibria $M_1 \leftrightarrow M_3$, which are shown in the time series in Figure 7c (bottom).

In the case under consideration, the stochastic system (3) demonstrates two-stage noise-induced transitions between two modes corresponding to states with different value of concentration x and almost equal values of temperature y. The first stage is the one-way transition from a larger value of the concentration to a smaller value ($M_3 \rightarrow M_1$), and the second stage (stochastic trigger) is intermittent behavior between these two concentration values ($M_1 \leftrightarrow M_3$).

The results of the statistical analysis in terms of the probability P of transitions are given in Figure 9 versus noise intensity ε for various values of the parameter D (the color matches the equilibrium from which we observe the transition). Here, we use the x-coordinate of the equilibrium M_2 as a threshold value. First, transitions from equilibria M_1 occur for higher levels of noise intensity ε. Second, for both equilibria, the following remark holds: the larger the value of D, the higher the required noise intensity for transitions.

3.2. Stochastic Effects in the Case 2 with $k_2 = 1$, $\gamma = 75$

Now, we consider stochastic system (3) with $k_2 = 1$, $\gamma = 75$ in the bistable parameter region $D_3 < D < D_6$ where the initial deterministic model exhibits a coexistence of two stable equilibria M_1 and M_3 (see Figure 3a). Figure 6a shows the x- and y-coordinates of the random states of the stochastic solutions starting at M_1 (green) and M_3 (blue) versus noise intensity for $D = 0.015$. First, as the noise increases, the dispersion of random states around both equilibria increases as well. For noise intensity $\varepsilon \approx 0.15$, solutions starting at M_1 (green) demonstrate transitions to M_3. In Figure 6b, these transitions are shown in terms of the mean values m_x, m_y of the stochastic states. For noise intensity $\varepsilon < 0.15$, the two mean values differ, but with further increases in ε, the mean values of the random states of the stochastic solutions starting at M_1 (green) rapidly increase and merge with the mean values for M_3 (blue). After this merging, both mean values slowly decrease. It is worth noting that in this case, only one-way noise-induced transitions $M_1 \rightarrow M_3$ are observed.

As in the previous case, when studying the noise-induced transitions, we will use the stochastic sensitivity function and method of confidence domains. Eigenvalues of the stochastic sensitivity matrix for equilibria M_1 (green) and M_3 (blue) are presented in Figure 12. For M_3, the largest eigenvalue is bigger than the eigenvalues for M_1. This is almost a constant for most of the interval $0 < D < D_6$ and only increases for $D > 0.032$. Eigenvalues for the equilibrium M_1 decrease as the parameter D moves to the right from D_3.

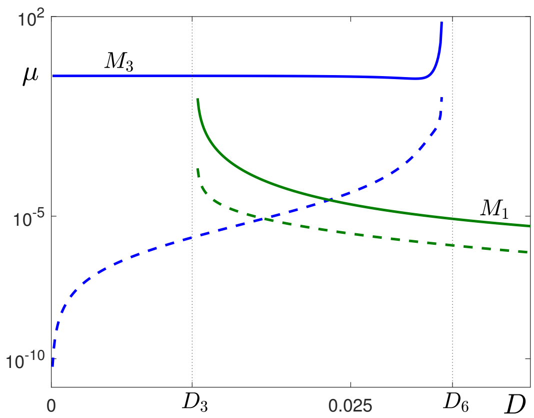

Figure 12. Eigenvalues μ_1 (solid) and μ_2 (dashed) ($\mu_1 > \mu_2 > 0$) of the stochastic sensitivity matrix of equilibria M_1 (green) and M_3 (blue) in stochastic system (3) with $k_2 = 1$, $\gamma = 75$.

Despite the fact that the sensitivity of the equilibrium M_3 is higher than sensitivity of the equilibrium M_1, and the spread of random states is larger around the equilibrium M_3, no transitions from M_3 to M_1 are detected. On the contrary, the transition from M_1 to M_3 occurs (see Figure 6). This fact can be explained by the following: the equilibrium M_1

is much closer to the separatrix (red dashed line) than the equilibrium M_3 (see Figure 8). In the top panels of Figure 8, we show confidence ellipses (black curves) around both equilibria for two values of the noise intensity. For $\varepsilon = 0.1$ (Figure 8a), both confidence ellipses do not intersect the separatrix. This means that random states are localized near equilibria M_1 or M_3, and transitions do not occur. This behavior is shown by the time series in Figure 8a, bottom. For $\varepsilon = 0.4$ (Figure 8b), one of the confidence ellipses, related to the equilibrium M_1, crosses the boundary of the basins of attraction. This indicates the occurrence of a noise-induced transition from M_1 to M_3. This transition is shown in the time series below.

So, in case 2, in contrast to case 1 described in 3.1, stochastic system (3) demonstrates only one-stage noise-induced transitions, namely from the mode with a lower value of concentration x and a larger temperature y to the mode with a larger value of concentration x and a smaller temperature y ($M_1 \to M_3$).

Details of the statistical analysis of these stochastic transformations are shown in Figure 10, where the probability P of transitions $M_1 \to M_3$ is plotted versus noise intensity ε for various values of the parameter D. Here, as before, we use the x-coordinate of the equilibrium M_2 as a threshold value. The larger the value of D, the higher the required noise intensity for transitions.

4. Conclusions

This paper is devoted to the problem of the mathematical modeling and computer simulation of complex nonlinear processes in the thermo-kinetics of autocatalysis. In our study, we considered a mathematical model of the dynamic interaction of reagent concentration and temperature. Parametric zones of bistability with the coexistence of two equilibrium regimes of thermo-kinetics were investigated. It was shown how random disturbances can deform deterministic dynamic regimes. When studying these noise-induced transformations, we applied the methods of direct numerical simulation with the subsequent statistical processing as well as the analytical stochastic sensitivity technique and apparatus of confidence domains. Two variants of bistability with different scenarios of stochastic transformations are studied and compared. The main result of this paper is a detailed analysis of noise-induced shifts in the probabilistic distributions of random states and probability of transitions from one equilibrium mode to another. For understanding underlying mechanisms of such transition, a key role of the mutual arrangement of basins of attractors, separatrices, and confidence ellipses is demonstrated. It is worth noting that this approach can be applied to the analysis of more complex stochastic models in various fields of science. The results presented in the paper shed light on the probabilistic mechanisms of the generation of complex oscillatory modes that appear in autocatalysis.

Author Contributions: Conceptualization, I.B. and L.R.; methodology, L.R.; software, T.P. and M.P.; validation, T.P., M.P. and I.B.; formal analysis, T.P.; investigation, T.P., M.P. and I.B.; resources, T.P.; data curation, M.P.; writing—original draft preparation, T.P. and I.B.; writing—review and editing, T.P. and I.B.; visualization, M.P.; supervision, L.R.; project administration, L.R.; funding acquisition, L.R. All authors have read and agreed to the published version of the manuscript.

Funding: This research was funded by the Ministry of Science and Higher Education of the Russian Federation (Ural Federal University Program of Development within the Priority-2030 Program).

Data Availability Statement: The data presented in this study are available on request from the corresponding author.

Conflicts of Interest: The authors declare no conflict of interest.

References

1. Schmidt, L.D. *The Engineering of Chemical Reactions*; Oxford University Press: New York, NY, USA, 1998.
2. Davis, M.E. *Fundamentals of Chemical Reaction Engineering*; McGraw-Hill: Boston, MA, USA, 2003.
3. Bykov, V.I.; Tsybenova, S.B.; Yablonsky, G. *Chemical Complexity via Simple Models*; De Gruyter: Berlin, Germany, 2018.

4. Uppal, A.; Ray, W.H.; Poore, A.B. The classification of the dynamic behavior of continuous stirred tank reactors—Influence of reactor resident time. *Chem. Eng. Sci.* **1976**, *31*, 205–214. [CrossRef]
5. Kawczyński, A.L.; Gorecki, J. Molecular dynamics simulations of sustained oscillations in a thermochemical system. *J. Phys. Chem.* **1992**, *96*, 1060–1067. [CrossRef]
6. Kawczyński, A.L.; Nowakowski, B. Master equation simulations of a model of a thermochemical system. *Phys. Rev. E* **2003**, *68*, 036218. [CrossRef] [PubMed]
7. Bashkirtseva, I.; Ivanenko, G.; Mordovskikh, D.; Ryashko, L. Canards oscillations, noise-induced splitting of cycles and transition to chaos in thermochemical kinetics. *Mathematics* **2023**, *11*, 1918. [CrossRef]
8. Shilnikov, L.P.; Shilnikov, A.L.; Turaev, D.V.; Chua, L.O. *Methods of Qualitative Theory in Nonlinear Dynamics*; World Scientific: Singapore, 1998; p. 416.
9. Guckenheimer, J.; Holmes, P. *Nonlinear Oscillations, Dynamical Systems, and Bifurcations of Vector Fields*; Springer: Berlin/Heidelberg, Germany, 1983; p. 462.
10. Kuznetsov, Y.A. *Elements of Applied Bifurcation Theory*; Springer: Berlin/Heidelberg, Germany, 1998.
11. Kloeden, P.E.; Platen, E.; Schurz, H. *Numerical Solution of SDE Through Computer Experiments*; Springer: Berlin/Heidelberg, Germany, 2002; p. 294.
12. Gautschi, W. *Numerical Analysis*; Springer: Berlin/Heidelberg, Germany, 2011.
13. Awrejcewicz, J. *Numerical Simulations of Physical and Engineering Processes*; InTech: Rijeka, Croatia, 2011; p. 614.
14. Butcher, J.C. *Numerical Methods for Ordinary Differential Equations*; Wiley: Chichester, UK, 2016; p. 544.
15. Milstein, G.N.; Tretyakov, M.V. *Stochastic Numerics for Mathematical Physics*; Springer: Berlin/Heidelberg, Germany, 2021; p. 736.
16. Bykov, V.; Tsybenova, S. A model of thermokinetic oscillations on the surface of a catalyst. *Russ. J. Phys. Chem. A* **2003**, *77*, 1402–1405.
17. Tsybenova, S. The basic thermokinetic models. *Phys.-Chem. Kinet. Gas Dyn.* **2008**, *6*, 281.
18. Bykov, V.; Tsybenova, S. A parametric analysis of the basic nonlinear models of the catalytic reactions. *Math. Model. Nat. Phenom.* **2015**, *10*, 68–83. [CrossRef]
19. Horsthemke, W.; Lefever, R. *Noise-Induced Transitions*; Springer: Berlin/Heidelberg, Germany, 1984; p. 338.
20. Anishchenko, V.S.; Astakhov, V.V.; Neiman, A.B.; Vadivasova, T.E.; Schimansky-Geier, L. *Nonlinear Dynamics of Chaotic and Stochastic Systems. Tutorial and Modern Development*; Springer: Berlin/Heidelberg, Germany, 2007; p. 535.
21. Arnold, L. *Random Dynamical Systems*; Springer: Berlin/Heidelberg, Germany, 1998; p. 600.
22. Lindner, B.; Garcia-Ojalvo, J.; Neiman, A.; Schimansky-Geier, L. Effects of noise in excitable systems. *Phys. Rep.* **2004**, *392*, 321–424. [CrossRef]
23. McDonnell, M.D.; Stocks, N.G.; Pearce, C.E.M.; Abbott, D. *Stochastic Resonance: From Suprathreshold Stochastic Resonance to Stochastic Signal Quantization*; Cambridge University Press: Cambridge, UK, 2008; p. 446.
24. Gardiner, C.W. *Handbook of Stochastic Methods for Physics, Chemistry and the Natural Sciences*; Springer: Berlin/Heidelberg, Germany, 1983.
25. Freidlin, M.I.; Wentzell, A.D. *Random Perturbations of Dynamical Systems*; Springer: New York, NY, USA; Berlin, Germany, 1984.
26. Mil'shtein, G.N.; Ryashko, L.B. A first approximation of the quasipotential in problems of the stability of systems with random non-degenerate perturbations. *J. Appl. Math. Mech.* **1995**, *59*, 47–56. [CrossRef]
27. Bashkirtseva, I.; Ryashko, L. Stochastic sensitivity of 3D-cycles. *Math. Comput. Simul.* **2004**, *66*, 55–67. [CrossRef]
28. Bashkirtseva, I.; Ryashko, L. Sensitivity and chaos control for the forced nonlinear oscillations. *Chaos Solitons Fractals* **2005**, *26*, 1437–1451. [CrossRef]
29. Ryashko, L.; Bashkirtseva, I.; Gubkin, A.; Stikhin, P. Confidence tori in the analysis of stochastic 3D-cycles. *Math. Comput. Simul.* **2009**, *80*, 256–269. [CrossRef]
30. Bashkirtseva, I.; Ryashko, L. Sensitivity analysis of stochastic attractors and noise-induced transitions for population model with Allee effect. *Chaos* **2011**, *21*, 047514. [CrossRef] [PubMed]
31. Bashkirtseva, I. Stochastic sensitivity analysis: Theory and numerical algorithms. *IOP Conf. Ser. Mater. Sci. Eng.* **2017**, *192*, 012024. [CrossRef]
32. Chen, J.; Zhang, T.; Zhou, Y. Stochastic sensitivity and dynamical complexity of newsvendor models subject to trade credit. *Math. Comput. Simul.* **2021**, *181*, 471–486. [CrossRef]
33. Bashkirtseva, I.; Perevalova, T. Analysis of stochastic bifurcations in the eco-epidemiological oscillatory model with weak Allee effect. *Int. J. Bifurc. Chaos* **2022**, *32*, 2250124. [CrossRef]
34. Bashkirtseva, I.; Ryashko, L. Sensitivity analysis of stochastically forced quasiperiodic self-oscillations. *Electron. J. Differ. Equ.* **2016**, *2016*, 1–12.
35. Bashkirtseva, I.; Ryashko, L. Stochastic sensitivity of the closed invariant curves for discrete-time systems. *Phys. A* **2014**, *410*, 236–243. [CrossRef]
36. Bashkirtseva, I.; Ryashko, L. Stochastic sensitivity of regular and multi-band chaotic attractors in discrete systems with parametric noise. *Phys. Lett. A* **2017**, *381*, 3203–3210. [CrossRef]
37. Alexandrov, D.V.; Bashkirtseva, I.A.; Crucifix, M.; Ryashko, L.B. Nonlinear climate dynamics: From deterministic behaviour to stochastic excitability and chaos. *Phys. Rep.* **2021**, *902*, 1–60. [CrossRef]

38. Slepukhina, E.; Bashkirtseva, I.; Ryashko, L.; Kügler, P. Stochastic mixed-mode oscillations in the canards region of a cardiac action potential model. *Chaos Solitons Fractals* **2022**, *164*, 112640. [CrossRef]
39. Bashkirtseva, I.; Chukhareva, A.; Ryashko, L. Stochastic dynamics of nonlinear tumor–immune system with chemotherapy. *Physica A* **2023**, *622*, 128835. [CrossRef]
40. Bashkirtseva, I. Method of stochastic sensitivity synthesis in a stabilisation problem for nonlinear discrete systems with incomplete information. *Int. J. Control* **2017**, *90*, 1652–1663. [CrossRef]
41. Bashkirtseva, I.; Ryashko, L.; Chen, G. Stochastic sensitivity synthesis in nonlinear systems with incomplete information. *J. Frankl. Inst.* **2020**, *357*, 5187–5198. [CrossRef]